Renewable and Sustainable Energy Reviews 93 (2018) 76–89

Contents lists available at ScienceDirect

Renewable and Sustainable Energy Reviews

journal homepage: www.elsevier.com/locate/rser

Energy-based metric for analysis of organic PV devices in comparison with conventional industrial technologies

Ana M. Gracia-Amillo*, Giorgio Bardizza, Elena Salis, Thomas Huld, Ewan D. Dunlop

Joint Research Centre, European Commission - Directorate C. Energy, Transport and Climate, Energy Efficiency and Renewable Unit, Via E. Fermi 2749 TP450, 21027 Ispra, VA, Italy

ARTICLE INFO

Keywords:
Organic photovoltaic devices
Energy rating
Photovoltaic performance
Module performance ratio

ABSTRACT

The emerging thin-film photovoltaic (PV) technologies show the potential to compete in the future market with the currently dominant crystalline silicon (c-Si) technology. A comparison of the different technologies based on their module performance rated at Standard Test Conditions (STC) is a commonly accepted method in the PV community. However, despite being a useful tool, it does not give enough information to accurately predict how much energy a PV module would deliver in the field when subjected to the wide range of real operating conditions.

In this paper we explore a potential screening method for new PV technologies; an energy-based metric to estimate the energy performance (Module Performance Ratio) of a PV module in a certain climate. This is constructed on the basis of validated models, and rigorous power rating measurements performed in controlled laboratory conditions at different temperature and irradiance levels. This method has the advantage that it can be applied to laboratory prototypes of technologies still in development as it does not require that the final product has reached maturity. The method has been applied to three thin-film PV technologies including the very innovative organic photovoltaics (OPV), and a comparison with c-Si is presented. The results obtained from the module performance ratio estimation in five different locations show how the emerging OPV technology performs similarly to some of the most common technologies considered and even outperforms slightly some technologies in some of the studied locations. These results could reinforce and support further development of this technology and its potential applications.

1. Introduction

Solar Photovoltaic (PV) technologies are today supplying about 1.5% of all the worldwide electricity demand [1] and generated €55billion revenue in 2015. Even though the market is dominated by crystalline silicon (c-Si) technologies, characterized by their high efficiency and long term stability, thin-film technologies (CdTe, CI(G)S, a-Si tandem etc.) make up around 10% of the share. Many research groups are developing alternative solar technologies with diverse properties and potential cost, environment and materials savings [2–5]. However, since the solar PV market is strongly expanding and the established conventional c-Si material continues to lead the way, the possibility to introduce new technologies is limited and a performance comparison with c-Si technology is compulsory.

In the last decade, a group of rapidly developing emerging PV technologies, such as organic photovoltaics (OPV), dye sensitized solar cells (DSSC) and perovskite solar cells (PSC) have entered the photovoltaics scene. They belong to the third generation of PV technologies according to the classification made by the European Photovoltaic Industry Association [6], while devices based on crystallite silicon wafers and the thin film inorganic semiconductor technologies constitute, respectively, the first and second generation. A detailed evolution of the market and development of these PV generations can be found in [7]. At present, there exist a few examples of products and prototypes of OPV and DSSC that are close to commercialization [8–10].

The efficiencies reached so far, although significantly lower than those of the multijunction devices or the well-established crystalline silicon based modules, are already comparable to those of other consolidated technologies, like amorphous silicon or some thin-film materials [11,12]. Considerable research effort on the said emerging technologies has addressed alternative approaches to increase their efficiency and reduce production costs by simplifying the manufacturing process, using new materials and reducing the amount and

* Corresponding author.
E-mail addresses: ana.gracia-amillo@ec.europa.eu (A.M. Gracia-Amillo), giorgio.bardizza@ec.europa.eu (G. Bardizza), elena.salis@ec.europa.eu (E. Salis), thomas.huld@ec.europa.eu (T. Huld), ewan.dunlop@ec.europa.eu (E.D. Dunlop).

https://doi.org/10.1016/j.rser.2018.04.029
Received 5 April 2017; Received in revised form 23 November 2017; Accepted 14 April 2018
1364-0321/ © 2018 Published by Elsevier Ltd.

cost of the required components [13–17]. However, there are some important drawbacks that restrain their commercialization, such as their relatively short lifetime and possible environmental impact [18–21]. This is particularly true for the case of perovskite solar cells which have reached a certified power conversion efficiency of 22% [3] but have stability problems [22–24] and may present potential toxicity and environmental effects [25,26].

The present study focuses on OPV devices based on semi-conducting polymers, which have been the topic of an increasing number of scientific publications during the last decades. Publications from the early 2000s have presented organic solar cells as a potential PV technology for the future despite the low efficiencies reported at the time [27,28], while more recent publications describe a wide range of materials used in OPV and document the increased efficiencies reached by this technology [29–34].

Compared to crystalline silicon devices, the distinct technical properties of the OPV devices could help them gain a niche in the PV market. Features such as low weight, mechanical flexibility and semi-transparency provide them some market opportunities since they could be easily integrated in architecture as building material or as urban furniture, as well as in portable devices [35]. The lower manufacturing costs of the roll-to-roll fabrication process compared to other technologies make them an attractive technology. Moreover, the efficiency of this developing technology has reached noticeable levels in a short period of time. From the reported efficiency of 3% in 2006 [36,37], cell efficiency has increased to more than 11% in 2015 [12,38]. Table 1 shows the confirmed efficiencies of OPV cells and minimodules compared with the values obtained by cells and submodules of some of the most common PV technologies. Data have been extracted from the most recent biannual report presented on certified efficiencies measured on solar cells and modules [12].

The efficiency values shown in Table 1 are reported at very specific conditions, defined as Standard Test Conditions (STC) [40], which are hardly ever met outdoors in real working situations. Thus, the efficiency really achieved by the PV devices under working conditions may differ substantially from these published values, since the performance of PV modules depends on many factors, like for example:

- The temperature of the module. For most technologies, the higher the temperature of the module is, the lower is its efficiency.
- The total incident solar irradiance, as depending on the physical structure of the solar cell the performance can be strongly dependent (and non-linear) with the varying solar radiation.
- The angle of incidence between the solar radiation and the normal to the module surface. In spite of the anti-reflective coating and the surface texture, as the angle of the incoming radiation increases, the proportion of reflected light increases, decreasing the energy available to be absorbed by the module.
- The spectral responsivity of the module's active material. Different materials may have different spectral responsivity to the range of wavelengths of the incoming irradiance, converting more efficiently some wavelength bands than others.
- The performance of some technologies may vary after long exposure to high irradiance levels or temperatures, while others may show seasonal effects on their energy production. This effect is not considered in the present study.

Table 1
Confirmed efficiencies of single-junction terrestrial cells and submodules measured under the global AM1.5 spectrum (1000 Wm^{-2}) at 25 °C (IEC 60904-3: 2008 [39], ASTM G 173-03 global).

Material	Efficiency (%)	Area (cm^2)
Organic (cell)	11.2 ± 0.3	0.992
Organic (minimodule)	9.7 ± 0.3	26.14
Si (crystalline cell)	26.7 ± 0.5	79.0
Si (amorphous cell)	10.2 ± 0.3	1.001
CdTe (cell)	21.0 ± 0.4	1.0623

Besides the intrinsic characteristics described above, others specifically related to the location and installation of the module also have an impact on the performance of a PV device. These are, for example, the orientation and inclination of the module, its location, possible shadows from the surrounding horizon, and presence of soiling or snow.

Studies about the performance of OPV devices under different working conditions are reported by different groups in literature. They are mainly focused on indoor measurements dedicated to the study of the positive effect of high temperatures which typically enhance the performance of OPV [41–44] and on outdoor measurements [45–52]. In these studies the behaviour of OPV devices at different irradiances and temperatures is analysed together with their long term stability. Most of these studies have been performed in northern Europe at high latitude locations (Denmark, Germany and Wales) although some other outdoor tests have been performed in other locations with higher levels of temperature and irradiance [53,54].

The objective of this paper is twofold: firstly, to analyse the performance of OPV devices under different climatic conditions in comparison to other technologies well established in the photovoltaic market, and secondly, to simultaneously validate the use of a PV power algorithm initially developed based on data of crystalline silicon modules, to estimate the PV production of organic devices.

Notwithstanding the estimation of the PV power values, the comparison between technologies is not based on these estimates but on the Module Performance Ratio (*MPR*) which is the ratio of the yearly output power and the received in-plane irradiation, for a PV array with a nominal power of 1 kWp. [55,56].

The algorithm applied to estimate the PV output, which is further described in [57], uses the temperature of the module and the in-plane irradiance as main input data. However, the complete methodology used to estimate the PV output also takes into account most of the effects that depend on the intrinsic characteristics of the PV technology, such as the temperature reached by the modules under working conditions, the spectral effects and the angle of incidence of the incoming radiation, both of which directly affect the effective in-plane irradiance, which is required as input data by the PV power algorithm. On the other hand, effects like shadows, degradation, ageing or presence of dust or snow are not considered in the present paper, as it is focused on the energy rating. This study does not aim at estimating the expected energy yield of the devices at real and specific locations, for which the latter effects and factors should be taken into account. Nevertheless, the methodology applied gives a good notion of how a PV technology would perform in a generic location and therefore is a good method to compare how different technologies would behave under the same conditions.

By using satellite-retrieved solar radiation data, we are able to estimate the PV output of the various considered technologies in several locations with very distinct climatic conditions. Furthermore, the spectrally resolved irradiance data enable taking into account the spectral impact on the performance of the PV devices which otherwise could not have been considered unless ground measurements had been available.

2. Input data

In the present study we have analysed four PV technologies: crystalline silicon (c-Si), cadmium telluride (CdTe), amorphous silicon (a-Si) and organic photovoltaics (OPV). Specifically, we used the following devices, named by the code used internally at the European Solar Test Installation (ESTI) laboratory: the PV modules TD81 (c-Si), KX712 (CdTe), CQ02 (a-Si), and one OPV mini-module (QJ87), all measured at ESTI laboratory of the European Commission. Their PV performance has been estimated at five different locations, whose latitudes range

Table 2
Coordinates of the five locations considered and optimal inclination angle applied at each of them.

Location	Latitude (°)	Longitude (°)	Optimal inclination angle (°)
Gabon	− 1.00	11.00	0
Saudi Arabia	24.91	46.41	25
Spain	38.00	− 3.25	34
Slovakia	48.00	18.00	36
Scotland	56.00	− 4.00	38

from 56°N to 1°S. The full analysis is based on one year of environmental data, 2011. The modules are assumed to be installed in a free-standing setting facing the equator with a fixed tilted angle with regard to the horizontal plane. In every location, the optimal inclination angle is applied so as to maximize the yearly received radiation at the module's surface. The optimal inclination angle, β_{opt} (°), calculated as described in [58], is shown in Table 2, along with the coordinates of the locations considered.

In order to estimate the PV output at the various locations with the models applied in this study, a number of different datasets are required.

2.1. Solar radiation data

The solar radiation data used in the present study has been retrieved from satellite images registered by the geostationary METEOSAT Second Generation Satellites located at 0° longitude. The data has been calculated with the SPECMAGIC algorithm, which is a spectrally resolved version of the MAGIC method (Mesoscale Atmospheric Irradiance Code). A detailed description of both algorithms can be found in [59,60]. Data has been calculated for the images registered in 2011, and one image per hour was processed in order to obtain the hourly dataset used in this study. The spatial resolution used is 3 arc-minutes, which correspond to approximately 5 km at nadir.

The satellite-based algorithm provides data of both the broadband global and beam irradiance on the horizontal plane, *G* and *Gb*, respectively, in Wm^{-2}. In addition to these values, the code output also contains data of the spectrally resolved irradiances integrated into 32 bands, the so-called Kato bands [61]. The covered wavelength range goes from 240 nm to 4605 nm. The bandwidth is not constant, since the bands were defined according to the spectral absorption and transmittance of the atmosphere's components. For this study, only bands 4–32 are considered, which cover the wavelength range from 306 nm to 4605 nm.

2.2. Ambient temperature and wind speed data

In order to apply some of the models required to estimate the PV production, data of wind speed, *Ws*, (ms^{-1}) and ambient temperature, T_{amb} (°C) is needed. These variables are extracted from the numerical weather forecast data produced by the European Centre for Medium-Range Weather Forecast (ECMWF) [62]. The hourly values used in the present study have been obtained by linear interpolation of the 3 h data available in the forecast product. The spatial resolution of the forecast data is 7.5 arc-minutes, which corresponds to around 14 km.

The wind speed in the ECMWF dataset represents wind speed at 10 m above ground. However, considering that most PV plants are located closer to ground level, the wind speed data was recalculated at 2 m elevation using Eq. (1).

$$Ws_m = \left(\frac{hm}{10}\right)^{0.2} \cdot Ws_{10} \quad (1)$$

Here Ws_m is the wind speed at the module's height, Ws_{10} is the wind speed at 10 m elevation as obtained from the forecast dataset, and *hm* is the module's height, assumed here to be 2 m. This is the same elevation considered by the forecast model to calculate the ambient temperature data.

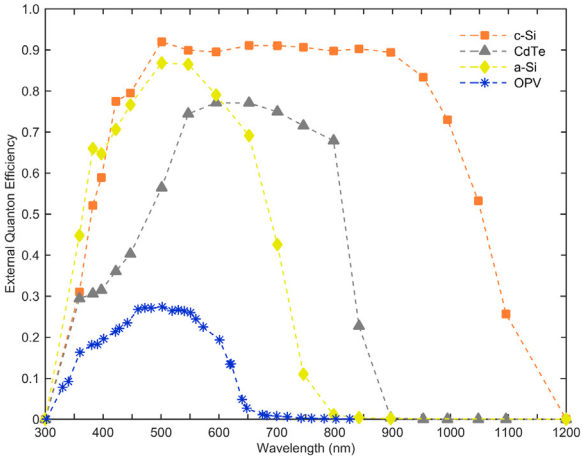

Fig. 1. External Quantum Efficiency curves for the four considered technologies, and devices used in every case: TD81 (c-Si), NW73 (CdTe), CQ02 (a-Si) and QJ87 (OPV).

2.3. Spectral responsivity data

The spectral responsivity (*SR*) measurements of the devices involved in the present study were performed at ESTI according to the standard [63]. The number of wavelengths included in each measurement depends on the technology and measuring setup used. For the OPV, 34 measurements were performed between 300 nm and 826 nm. For the other three technologies, the number of measurements varies between 16 and 20 covering the range between 300 nm and 1200 nm. Further information about how these measurements were acquired is given in [64–66].

Fig. 1 shows the comparison between the External Quantum Efficiency (*EQE*) values of the devices described in Section 2. An exception has been done for the CdTe technology for which the SR of the module NW73 is shown, instead of the KX712, because the former was used in the spectral mismatch calculations. Since the two CdTe modules have very similar *SR* values, it has been possible to combine the *SR* data of the NW73 with the power matrix data of the KX712 without significantly affecting the performance evaluation of this technology. The *EQE* is calculated from the *SR* measurements following Eq. (2).

$$EQE(\lambda) = \frac{1239.8}{\lambda} \cdot SR(\lambda) \quad (2)$$

Here λ is the wavelength, in nm, at which the *SR* data point was measured. The *EQE* is a dimensionless parameter that quantifies the efficiency of a PV device in converting the energy of the incoming photons. In the ideal case, the energy from every single incoming photon would be fully converted into electricity collected at the PV device terminals and the *EQE* would be equal to 1.

2.4. Matrix of PV output measurements registered at different levels of in-plane irradiance and module temperature

The power output at the maximum power point (P_{max}) produced by the PV devices was measured, under indoor controlled conditions, at different levels of irradiance perpendicular to the module surface, G_n, (Wm^{-2}) and module temperature, T_{mod} (°C). The measured irradiance and temperature intervals, as well as the steps used for each variable, vary with the technology, as shown in Table 3. For every level of irradiance, P_{max} was measured at various levels of module's temperature.

At every measurement setting, combination of the G_n and T_{mod} values applied, at least three measurements were taken for every

Table 3
Indoor measurement setting applied to each device.

Device	Irradiance (Wm^{-2})	Module temperature (°C)	N of data points
TD81 (c-Si)	100, 200, 400, 600, 800, 1000	25, 35, 45, 60	24
KX712 (CdTe)	100, 200, 300, 400, 500, 600, 700, 800, 900, 1000	25, 35, 45, 55	40
CQ02 (a-Si)	100, 200, 300, 400, 500, 600, 700, 800, 900, 1000	25, 35, 45, 55	40
QJ87 (OPV)	100, 200, 400, 600, 800, 1000	15, 20, 25, 30, 35, 40, 45	42

technology. So, the P_{max} values used in the present analysis are in fact, the average of those. The final number of data points contained in the PV power matrix is shown in Table 3.

A detailed description of the procedure applied to obtain the power matrix for the OPV device can be found in [66]. For the other three technologies, the power matrix data used in the present study are described in [67,68].

The irradiance range covered is the same for the four technologies, although the number of intermediate points is larger for the CdTe and a-Si technologies. Regarding the module temperature, the maximum power was measured at different values covering a total range of 30 °C or 35 °C depending on the device. The temperature values set for the OPV device are lower than those applied to the other three technologies in order not to risk provoking change or degradation during the measurements.

3. Methodology

The model used for the estimation of the PV power output uses various input values that, in turn, have to be estimated on the basis of the available data described in Section 2. Therefore, the complete methodology is a concatenation of different models that are described in the present section.

3.1. Estimation of the in-plane irradiance

The irradiance data retrieved from the satellite-based model, both broadband and spectrally resolved values, are estimated for the horizontal plane. Since, in this study, the modules are tilted at the optimal inclination angle, β_{opt} (°), the irradiance on this tilted plane has to be estimated for every location and hour. The method used in this case is the one developed by Muneer [69], which has been shown to compare well to other methods [70]. It was applied to obtain the global broadband irradiance values (G_T) and the global spectral irradiance ($G_{T,\lambda}$) values integrated in the Kato bands 4–32. The corresponding values of the beam component are calculated as well (Gb_T and $Gb_{T,\lambda}$).

3.2. Estimation of the in-plane irradiance corrected for Angle-Of-Incidence effects

The Angle-of-Incidence (AOI) effect accounts for the reduction in the impinging irradiance that is transmitted to the module's photoactive material, due to increased reflection at the module's surface when the light arrives at an angle different from perpendicular. The model used to account for this effect is the one developed by Martín and Ruiz [71,72]. The model applies different equations to the two components of solar irradiance. Eq. (3) is for estimating the beam component corrected for AOI effects (Gb_{T_AOI}). While Eq. (4) is used for the diffuse irradiance, which is considered isotropic, (Gd_{T_AOI}). The global irradiance is the sum of both components (Eq. (5)). The same equations have been applied to estimate the broadband (G_{T_AOI}) and the spectrally resolved (G_{T,λ_AOI}) irradiance values at every considered Kato band.

$$Gb_{T_AOI} = Gb_T \cdot \left(\frac{1 - \exp\left(\frac{-\cos\delta}{a_r}\right)}{1 - \exp\left(\frac{-1}{a_r}\right)} \right) \tag{3}$$

$$Gd_{T_AOI} = Gd_T \cdot \left(1 - \exp\left[\frac{-1}{a_r} \cdot \left(\frac{4}{3\pi}\left(\sin\beta + \frac{\pi - \beta - \sin\beta}{1+\cos\beta}\right) + (0.5 \cdot a_r - 0.154) \cdot \left(\sin\beta + \frac{\pi - \beta - \sin\beta}{1+\cos\beta}\right)^2\right)\right]\right) \tag{4}$$

$$G_{T_AOI} = Gb_{T_AOI} + Gd_{T_AOI} \tag{5}$$

Here δ is the angle of incidence between the direct sunlight and the normal to the module's surface and β is the inclination angle of the module, in radians. This is the optimal inclination angle for every location, β_{opt}. a_r is the angular losses coefficient, a dimensionless parameter that has to be determined for every module's type of encapsulation. For the present study a value of $a_r = 0.155$ was used [71].

3.3. Estimation of the in-plane irradiance corrected for spectral effects

The spectral responsivity is an intrinsic characteristic of the PV devices, as shown in Section 2.3. Thus, under the same conditions of broadband irradiance and spectrum, different PV technologies may provide different energy output, due to their specific sensitivity to the different wavelengths.

The spectral effect can also be observed in the output of the same module at different times. Considering the device's performance under very specific conditions, such as the STC, assuming that only the spectral distribution changes from the reference spectrum [39], maintaining constant the total irradiance and the module temperature, a deviation in the maximum power from the corresponding STC value would still be observable. This effect is considered in the spectral mismatch factor, *MM*, as defined by the standard IEC 60904-7 [73], and simplified here according to Eq. (6).

$$MM = \frac{\int SR(\lambda) \cdot R(\lambda) d\lambda}{\int SR(\lambda) \cdot R_{STC}(\lambda) d\lambda} \cdot \frac{G_{T,STC}}{G_T} \tag{6}$$

$SR(\lambda)$ is the spectral responsivity value at wavelength λ. $R(\lambda)$ is the spectral irradiance at wavelength λ, while $R_{STC}(\lambda)$ is the spectral irradiance at wavelength λ of the STC spectrum [39]. G_T and $G_{T,\ STC}$ are, respectively, the in-plane broadband irradiance at the considered moment and that of the STC spectrum.

Since the spectrally resolved irradiance data retrieved from satellite is integrated in discrete bands, Eq. (6) is applied to these bands, not to single wavelengths. In order to do so, the measured $SR(\lambda)$ values are interpolated at the central wavelength of every Kato band. The resulting *SR* values are assumed to be constant for all the wavelengths inside every band. The STC spectrum is also split according to the Kato bands, so the same spectral responsivity values are applied to it. The STC spectrum $R_{STC}(\lambda)$ is scaled so that the integral STC irradiance is the same as the broadband irradiance G_T.

Thus, after correcting for AOI effects, the spectral effects are also taken into account (Eq. (7)), giving an estimate of the effective in-plane irradiance, G_{T_eff}, that is available for the module to be used in the PV production.

$$G_{T_eff} = G_{T_AOI} \cdot MM \tag{7}$$

3.4. Estimation of the module temperature

Although the variable that most significantly affects the PV output is the effective in-plane irradiance received by the modules, the temperature of the device can also play an important role in the final output. The way the performance is affected by the temperature

Table 4
Coefficients u_0 and u_1 used for the estimation of T_{mod}.

	c-Si	CdTe	a-Si
u_0 (W/°C m^2)	26.91	23.37	25.71
u_1 (W s/°C m^3)	6.2	5.44	4.26

depends on the technology, although in most cases the PV power drops with increasing temperature.

In the present study, the temperature of the module is estimated by means of the model developed by Faiman [74], whose main expression is shown in Eq. (8). Like most models [75] it considers the temperature increase due to the ambient temperature and the received irradiance, but it also models the cooling effect of the wind which is often neglected due to the lack of data despite its proven effect on the temperature of the module [76]. The input parameters are the Ws (ms^{-1}) and the T_{amb} (°C) at 2 m elevation, together with the in-plane irradiance, only corrected for the Angle-Of-Incidence effects.

$$T_{mod} = T_{amb} + \frac{G_{T_AOI}}{u_0 + u_1 \bullet Ws} \tag{8}$$

The two coefficients u_0 and u_1 depend on the technology and on the way the modules are mounted (freestanding, roof-mounting, building integrated). The values considered in the present study, shown in Table 4, are for a free-standing rack and are extracted from [77].

Since these coefficients haven't been defined for the OPV technology, it was decided to apply those of the c-Si and also those for the CdTe, in order to analyse the effect that this variable would introduce in the module energy output.

3.5. Estimation of the PV power

The model used to estimate the PV performance [57] considers the module's power as a function of the received irradiance and the temperature of the module. Although originally developed for modelling c-Si modules, it has been used for other technologies with good results [78]. In the present paper, we analyse whether it is suitable or not for modelling the OPV devices' performance. The general mathematical expression of the model follows Eqs. (9) to (11).

$$P(G',\ T') = G' \bullet P_{STC} \bullet (1 + k_1 \ln(G') + k_2 (\ln(G'))^2 + k_3 T' + k_4 T' \ln(G') + k_5 T' (\ln(G'))^2 + k_6 (T')^2) \tag{9}$$

$$G' = G / G_{STC} \tag{10}$$

$$T' = \mathrm{T_{mod}} - T_{STC} \tag{11}$$

Here, G is the in-plane irradiance received by the module. If the effects described in the previous Sections 3.2 and 3.3 (AOI and spectral effects) are taken into account, G would be the effective in-plane irradiance available to the module (G_{T_eff}).

G_{STC} and T_{STC} are, respectively the STC irradiance (1000 Wm^{-2}) and temperature (25 °C). P_{STC} is the module's maximum power referred to STC.

The coefficients k_1 to k_6 are defined by fitting Eq. (9) to the measured data described in Section 2.4. This fit was performed on the data for the four modules. In each case, the power was normalized so that P_{STC} = 1 Wp before the fit was performed. The coefficients obtained for the four considered technologies are given in Table 5.

3.6. Module performance ratio

With the models described above it is possible to estimate, for every hour of the time series, the temperature of the module (T_{mod}) and the effective in-plane irradiance (G_{T_eff}). With these variables, the expected PV output can be calculated at every location by means of Eq. (9). However, the comparison between the different PV technologies is not focussed on the hourly PV output values but on the Module Performance Ratio (*MPR*), calculated according to Eq. (12) [79]. This value gives an idea of the overall performance of every technology over the time period considered. In this paper we have calculated both the yearly and the monthly values (*MPRy* and *MPRm*, respectively).

$$MPR = \frac{\sum PV\ output}{\sum G_T} \bullet \frac{G_{STC}}{P_{STC}} \tag{12}$$

Depending on the time period considered, yearly or monthly, the sum of the corresponding hourly values is applied. In this case, the value of G_T is the inclined irradiance as calculated with Muneer's model. That is to say, without applying any correction for angle of incidence or spectral effects. These effects are however considered in the irradiance values used to estimate the PV output, (G_{T_eff}).

3.7. Variations in the PV output estimation

The PV output is calculated using the model developed by Huld et al. (Eq. (9)) which has been applied successfully to estimate the performance of various PV technologies. In addition to this, the model was compared to others with consistent results between the approaches [78]. However, until now it had not been applied to model OPV devices.

A first approach to validate the model for this technology is by comparing the results obtained from Eq. (9) using the same in-plane irradiance and module temperature conditions used in the measurements described in Table 3 and the measured data themselves. The estimated values should be very similar to the P_{max} values of the measured matrix, since the coefficients k_1 to k_6 used in Eq. (9) are obtained by fitting the equation to the 42 measured points. However, this will give little information about the ability of the model to predict the energy output.

In order to increase the number of points used to assess the suitability of the model equation for OPV, the PV output is calculated for all the occurrences of the time series described in Sections 2.1 and 2.2 (hourly values for 2011) for which the estimated values of G_{T_eff} and T_{mod} are inside the intervals measured in the power matrix. This means that only the occurrences when G_{T_eff} falls between 100 Wm^{-2} and 1000 Wm^{-2} and T_{mod} is between 15 °C and 45 °C will be considered. For those occurrences, the PV output is estimated in two different ways: on the one hand, applying Eq. (9) and, on the other hand, using a linear interpolation to the values of the measured matrix following [55].

When limiting the considered occurrences to those that comply with the irradiance and module temperature intervals measured in the PV matrix (Table 3), there is a considerable number of hours within the

Table 5
Coefficients for the PV performance model for every technology considered.

Technology	k_1	k_2	k_3	k_4	k_5	k_6	Normalized P_{STC}
c-Si	0.015391	− 0.028551	− 0.003970	− 0.000081	0.000080	− 0.000007	1.0000
CdTe	− 0.046689	− 0.072844	− 0.002262	0.000276	0.000159	− 0.000006	1.0000
a-Si	− 0.138372	− 0.099818	− 0.000155	0.001511	0.000497	− 0.000057	1.0129
OPV	− 0.071407	− 0.180987	0.001772	0.001587	0.000918	− 0.000075	1.0018

Table 6
Differences in % between the yearly sum of PV power values from methodologies 'Matrix' and 'Equation_limited' on the left side and 'Matrix_extended' and 'Equation' on the right side.

	'Matrix' vs 'Equation_limited'				'Matrix_extended' vs 'Equation'			
Location	c-Si	CdTe	a-Si	OPV	c-Si	CdTe	a-Si	OPV
Gabon	0.52	0.17	− 1.20	0.76	− 0.08	0.16	− 0.27	0.85
Saudi Arabia	0.43	0.13	− 0.35	0.07	− 0.06	0.13	0.98	1.22
Spain	0.35	0.11	− 0.35	0.02	− 0.04	0.15	0.41	1.13
Slovakia	0.35	0.10	− 0.46	0.07	0.10	0.19	− 0.49	1.19
Scotland	0.28	0.04	− 1.05	0.15	0.14	0.16	− 1.91	2.08

time series that are dismissed, especially in those locations at low latitudes where the module may become very hot. In order to analyse the module performance under all possible conditions, all the yearly data must be considered. This does not raise any problem when applying the model equation. However, the interpolation procedure is not applicable anymore as there are no measured P_{max} values that cover all the environmentally observed conditions, since laboratory verified matrix measurements are restricted to the intervals shown in Table 3.

To overcome this problem, the original data of the PV matrix were supplemented with new values obtained by extrapolation of the measured ones, so as to cover all the possible conditions of irradiance and temperature recorded in the five locations. The initial in-plane irradiance interval was increased to cover the range from 50 Wm^{-2} to 1200 Wm^{-2}, while the module temperature range was increased from − 15 to 100 °C. Unlike the uneven steps applied in the measured matrices, in this extended case constant steps of 50 Wm^{-2} and 5 °C were applied. As a result, the extended matrix has PV output values at 50 Wm^{-2}, 100 Wm^{-2}, 150 Wm^{-2} up to 1200 Wm^{-2}, and from − 15 °C to 100 °C at 5 °C steps. Doing so, the number of points was increased to 576. The procedure used to obtain the extended matrix is described in the Annex to this paper.

As a result, we have applied four different methodologies to estimate the PV output from the four technologies at the five different locations. The four different methodologies are defined as follows:

1. 'Matrix'. Applied to the occurrences whose in-plane effective irradiance and temperature of the module values are inside the initial intervals considered in the PV matrix described in Table 3. The PV output values calculated with this 'Matrix' methodology are the linearly interpolated values obtained from the power values of the initial matrix.
2. 'Equation_limited'. With this methodology the PV performance model (Eq. (9)) is only applied to those hours when the G_{T_eff} and the T_{mod} fall inside the initial intervals of the PV matrix.
3. 'Matrix_extended'. With this methodology all the hourly values in the time series can be considered. And the PV output is estimated as interpolation of the power values of the extended matrix.
4. 'Equation'. Eq. (9) is applied to all the hourly values in the time series.

Methodologies 'Matrix' and 'Equation_limited' consider the same moments and their comparison is useful to assess the use of the Eq. (9) to model the performance of other technologies other than the c-Si, which was the original aim of the model.

Similarly, methodologies 'Matrix_extended' and 'Equation' work with the same number of points, all the yearly values of the time series, and their results are comparable. The only limitation considered in this case is that the PV output is set to 0 for those moments when the G_{T_eff} is below 50 Wm^{-2} or above 1200 Wm^{-2}.

4. Results and discussion

The present study pursues two main objectives. One of the objectives is to validate the power model (Eqs. (9)–(11)) for the estimation of the PV power generated by other technologies than the c-Si, paying special attention to OPV. And the other main objective is to estimate the performance of this organic technology in different climatic regions and to compare it to other technologies well established in the PV market.

4.1. Differences in the PV power estimates from the PV model and the interpolation methodologies

The suitability of the PV power model [57] is to be assessed by comparing the estimated values (Eq. (9)) to real PV power measurements. However, due to the reduced number of available measurements (Table 3), the model's estimates are compared to the values obtained by methodologies 'Matrix' and 'Matrix_extended'. In the first case, the values obtained come from the interpolation of the real PV power data, which were also used to obtain the equation's coefficients (k_1 to k_6). The 'Matrix_extended' methodology relies on extrapolated values outside the boundaries considered in the initial PV power matrix.

When the comparison is limited to the hours whose G_{T_eff} and T_{mod} values are inside the intervals of the original measured matrix, the sum of the PV power interpolated values of the 'Matrix' methodology are higher than those calculated by Eq. (9) for all technologies but the a-Si, for which the estimated PV power from 'Equation_limited' are between 0.35% and 1.2% higher than the 'Matrix' ones, depending on the location. The differences are in general smaller for the other three technologies, especially for the OPV. The low differences between the output PV power from these two methodologies, in the order of 0.4% or less in most cases, support the validation of the power model to estimate the performance of other PV technologies besides c-Si, including OPV. In fact, except from the results observed at latitudes 1°S and 56°N, where differences are 0.76% and 0.15% respectively, in the other three locations the PV power values for OPV differ in less than 0.1%, as shown in Table 6. The differences are below 0.2% for the CdTe technology, while for the silicon based ones, the deviations are higher.

When all the hourly values are considered ('Matrix_extended' and 'Equation'), the differences in the yearly sum of PV power obtained from both methodologies do not change significantly with regard to the limited analysis ('Matrix' and 'Equation_limited') for the CdTe technology. On the contrary, for the c-Si technology, differences are considerably reduced. As for the other two technologies, differences increase, especially for the organic device. The yearly sum of PV power estimated for the organic device by the power model can be up to 2% lower than the value retrieved from the 'Matrix_extended' methodology. The opposite is observed for the a-Si technology, for which the model tends to provide higher power values than the matrix based methodology.

The highest deviations for the various technologies, except CdTe, are observed in Scotland, where there is a high occurrence of low irradiance values, mostly excluded in the first comparison ('Matrix' against 'Equation_limited'). At this location, the percentage of daytime hours with an in-plane irradiance below 200 Wm^{-2} is 28%, while it is 21% for the location at 48°N and 14% for the location at 1°S. The larger

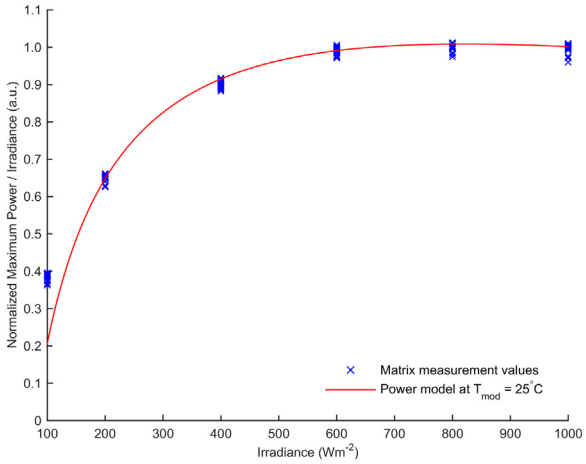

Fig. 2. Maximum power data extracted from the I-V curves of the measured power matrix for QJ87 (OPV) and normalized to 1 at 1000 Wm^{-2} (crosses). One fitting curve of the power model (Eq. (9)) with T_{mod} of 25 °C has been plotted as example for comparison (red line) (For interpretation of the references to color in this figure legend, the reader is referred to the web version of this article.).

difference between the OPV results by 'Matrix_extended' and 'Equation' at sites with a high incidence of low irradiance conditions may be due to the imperfect fit of the model to those conditions, as shown in Fig. 2. Fig. 2 plots the normalized maximum power for the OPV device when applying the power model with the coefficients shown in Table 5 and a module temperature of 25 °C, against the maximum power data extracted from the I-V curves measured in laboratory (Table 3), and normalized to 1 at 1000 Wm^{-2}. At low irradiance levels discrepancies between the calculated values and the measurements increase.

The larger differences obtained when all the yearly time series is considered, for the a-Si and OPV technologies in comparison to the other two, might be due to a non-linear dependence of these devices' PV output to the irradiance and temperature values. The algorithm's coefficients k_1 to k_6 are obtained by fitting the equation to the PV power measurements described in Section 2.4 where low irradiance cases were not applied. Under those circumstances, the linearly extrapolated PV power values tend to disagree with the algorithm's estimates.

A new adjustment of the model's coefficients using more PV power measurements registered at additional conditions of irradiance and temperature could refine the model's estimates and help reducing the differences reported in Table 6. For this aim, new PV power measurements at low irradiance levels would be very valuable. Notwithstanding, the reported differences between the power output from 'Matrix' and 'Equation_limited' do not indicate the need to modify the power model in order to be applied to other technologies different from the c-Si one.

4.2. Module performance ratio

One of the main objectives of the present paper is the estimation of the performance of the organic device in different locations and analyse how it compares to other technologies. This comparison is based on the Module Performance Ratio (Eq. (12)).

4.2.1. Yearly MPR

Looking at the yearly *MPR* values, the a-Si technology has the highest values for all the locations (see Fig. 3) with the exception of location at 24°N when all the hourly values in the entire time series are considered ('Equation' and 'Matrix_extended'). In this case, the OPV outperforms the other technologies with *MPR* values slightly higher than the one obtained with the a-Si. However, regardless of the methodology applied, the OPV has the lowest *MPR* at the highest latitude, as can be seen in Fig. 3, although, in general, the lowest *MPR* are obtained for the c-Si technology.

Excluding the occurrences with low in-plane irradiance values from the calculations ('Equation_limited' and 'Matrix' methodologies dismiss any moment below 100 Wm^{-2}) results in higher *MPR* values, especially at the locations where these cases are more frequent. This is especially remarkable for the organic technology at latitudes 56°N and 48°N, whose *MPR* values decrease considerably when all the time series is considered ('Equation' and 'Matrix_extended').

4.2.2. Monthly MPR

The monthly *MPR* values were also calculated (see Fig. 4). Only the results from methodologies 'Matrix_extended' and 'Equation' are presented as they take into consideration the whole time series providing a more complete overview of the performance of the different technologies under real working conditions. Note that seasonal variations in the STC power of the modules are not considered in this study.

The monthly *MPR* values resulting from the equation (*) and from the interpolation procedure (line) are very similar for the c-Si and CdTe technologies in all the five locations. This supports the use of the model to estimate the performance of the CdTe technology also under the conditions that are outside the range used in the original measured power matrix described in Section 2.4.

Differences between the *MPR* values from the 'Equation' and 'Matrix_extended' methodologies are more significant for the other two technologies, especially at lower latitudes. For the OPV device, the 'Equation' tends to result in lower *MPR* values than the 'Matrix_extended', while there is not a clear trend for the a-Si, since none of the two methodologies provides higher *MPR* values in all the locations or months.

The model was originally developed for c-Si [57] and then also validated for CdTe [78]. The good correlation between the output from 'Equation' and 'Matrix_extended' shows that the performance of these two technologies is more linear than the other two technologies with regard to the temperature of the module and the in-plane irradiance, as the extended matrix was obtained by linear interpolation and extrapolation of the measured values used to calculate the coefficients of the model. These coefficients, though, need further adjustment for the other two technologies, since the output of 'Equation' and 'Matrix_extended' do not agree so satisfactorily. Alternatively this could indicate that the performance of the measured devices is not so linear with regard to T_{mod} and to G_T as the other two technologies.

The a-Si technology tends to perform better than the other technologies. However, the OPV has higher *MPR* values than the a-Si technology in conditions of blue-richer spectra or in summer months, with the exception of the location at 56°N where it performs worse than any other technology. The OPV performance tends to decrease in winter months, more significantly as latitude increases. The c-Si and CdTe show a relatively constant behaviour during the year for the location at 1°S, and at latitudes above 48°N. On the other hand, in the intermediate latitudes, their performance decreases during summer months due to the increased temperature of the module. The monthly *MPR* values of the a-Si technology are quite stable through the year, with a small decrease during the winter months at the highest latitudes. The monthly evolution of the estimated *MPR* values follow the same trend observed in real PV performance measurements recorded during real outdoor working conditions of the inorganic technologies considered in the present paper [80,81] which supports the methodology presented. Since degradation is not considered, real outdoor performance of OPV devices reported in literature cannot be compared to the values obtained here.

In the monthly *MPR* values shown in Fig. 4 for the location near the equator (Gabon), there is a remarkable decrease in the OPV values for the central months. The values shown so far for the OPV were obtained calculating the temperature of the module with the Faiman model coefficients u_0 and u_1 of the c-Si technology, so T_{mod} is the same for both

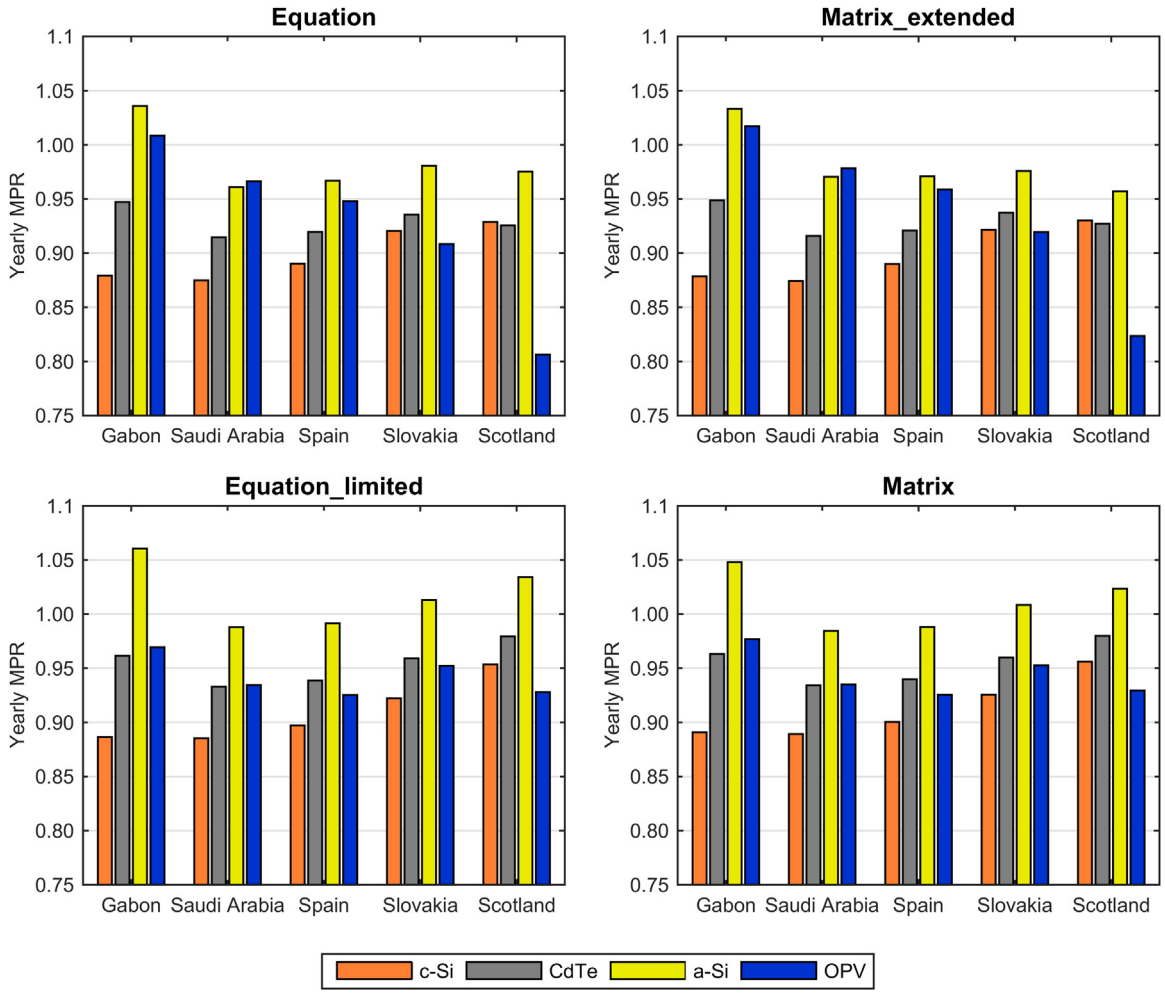

Fig. 3. Yearly *MPR* values derived from the four applied methodologies at the five different locations.

technologies. Since the modules also have the same setting, the angle of incidence effects are also the same. So, the different behaviour of the organic and the c-Si technologies shown in Fig. 4 could derive from the spectral effects or from the intrinsic behaviour of these technologies under the conditions of temperature and irradiance observed at that location.

The spectral effects can be quantified by the mismatch factor (Eq. (6)). For the OPV device, at this location, the monthly *MM* varies between 1.126 and 1.172 (12.6–17.2%), whilst for the c-Si technology it goes from 1.036 to 1.052 (3.6–5.2%). This effect is homogeneous through the year for both technologies, more so for the c-Si. Therefore it does not seem enough to explain the reduced *MPR* observed for the OPV device during the period between June and August. However, analysing the monthly values of the ratio between the PV output and the G_{T_eff}, which includes AOI and spectral effects, there is more variability for the OPV device. For c-Si, it is between 0.875 and 0.898, while for the OPV it can change between 0.861 and 0.955. The lower values of this ratio are observed during the central months when T_{mod} and G_T also decrease at this location. Table 7 contains the average monthly values during daytime of the in-plane irradiance, G_T, the temperature of the module (the same for the organic and the c-Si devices), the effective irradiance, G_{T_eff}, and the power output observed in January and June for the location near the equator for the OPV and the c-Si technologies. The ratio of the latter two parameters is also calculated.

The value of the ratio between the PV output and the effective in-plane irradiance of the organic device in June is approximately 10% lower than in January. In contrast, the estimated ratio for the c-Si changes only by about 1%. At the low irradiance conditions observed during the central months at this location, like in June, the OPV technology performs significantly worse than during the rest of the year.

This poor performance delivered by the organic device under low irradiance conditions is noticed as well at high latitudes when the occurrence of low irradiance levels is high, especially in winter months. In fact, if we compare the monthly *MPR* values obtained from the four methodologies, the *MPR* values from 'Matrix' and 'Equation_limited', which dismiss the hours with irradiance below 100 Wm^{-2}, are higher. Including these low in-plane irradiance moments strongly reduces the *MPR* values for both technologies, especially for the organic one for which the reduction of the *MPR* can be of up to 60% as in December, when the *MPR* passes from 80% to 35% approximately. Fig. 5 contains the monthly *MPR* values from the four methodologies estimated for the location furthest north for the organic and the c-Si technologies. The range of T_{mod} measured in the initial matrix (Table 3) explains why there are no *MPR* values for December or January from 'Matrix' or 'Equation_limited' for the c-Si technology as the temperature of the c-Si module never reaches 25 °C.

4.3. Further analysis of different effects

In this section we analyse in more detail the impact of some variables on the final *MPR* values. In the first place we analyse the implications of extending the analysis to situations outside the controlled conditions measured indoors. We then analyse the impact of the effects taken into consideration in the PV power model: AOI, spectral effects

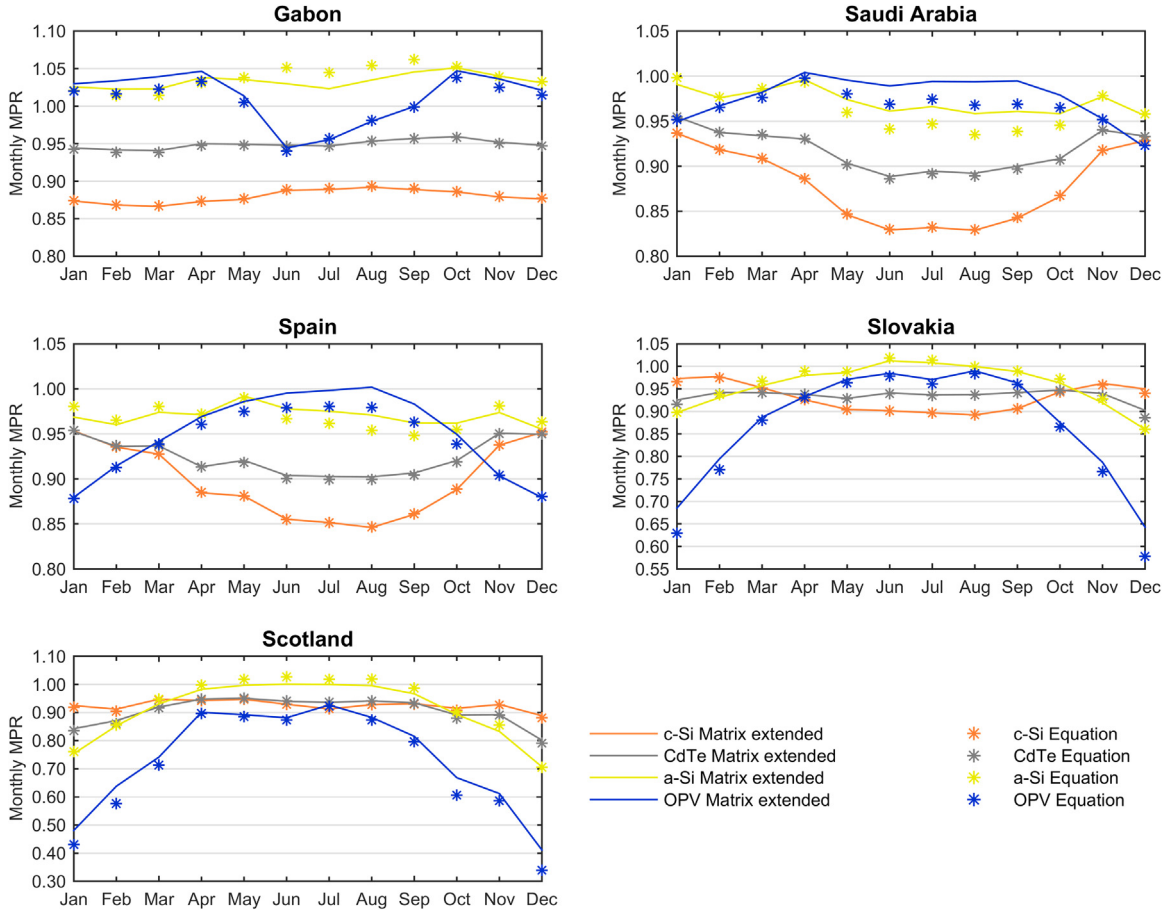

Fig. 4. Monthly *MPR* of the four technologies at the five considered locations. Only 'Equation' and 'Matrix_extended' are shown. Note the different ranges covered in the Y-axis.

and module's temperature.

4.3.1. Analysis limited to the conditions measured indoor

The monthly *MPR* values shown in Fig. 4 were obtained using the whole time series of hourly values from 2011. The T_{mod} and G_{T_eff} values of some hours fall outside the (G, T) ranges of the initial matrix, so the PV output estimated in those cases with the 'Matrix_extended' methodology relies on extrapolated values. These are, in some cases, based on interpolated values, since the measured values of temperature and in-plane irradiance are fewer and at larger steps than those calculated in the extended matrix. (See the Annex and Section 3.7). Both extrapolation and interpolation procedures may introduce errors in the estimate of the PV output, especially for technologies with a non-linear behaviour with G and T for which the indoor measurements were taken at dispersed intervals like 200 Wm^{-2} or 10 °C.

Therefore, it is interesting to quantify how much of the estimated yearly PV production comes from hours whose (G, T) conditions are within those of the measured power matrices and how much relies on extrapolated values.

Since the (G, T) measured ranges vary between the technologies, the

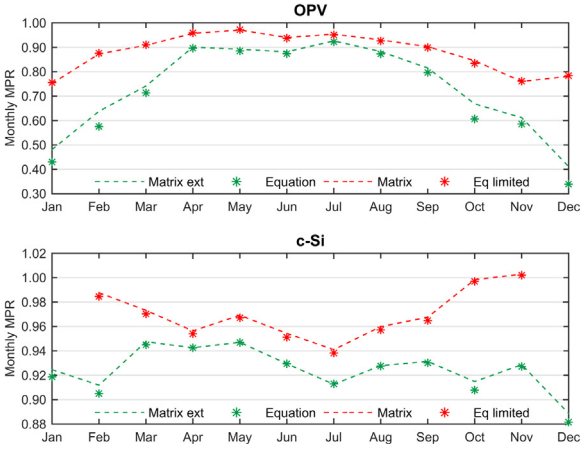

Fig. 5. Monthly *MPR* values at the location 56°N for the organic and the c-Si technologies obtained by applying the four methodologies.

Table 7
Performance of the OPV and c-Si technologies in January and June in the location at 1°S. The values shown here are the monthly averages during daytime.

			OPV			c-Si		
	G_T (Wm^{-2})	T_{mod} (°C)	G_{T_eff} (Wm^{-2})	PV output (W)	Ratio (m^2)	G_{T_eff} (Wm^{-2})	PV output (W)	Ratio (m^2)
January	472	40	511	487	0.953	466	412	0.883
June	292	33	321	276	0.860	290	260	0.891

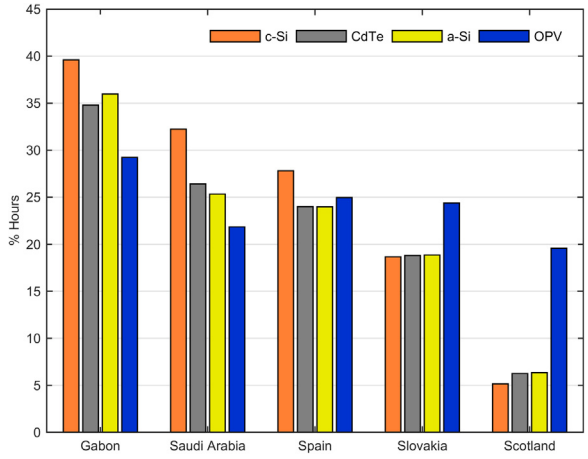

Fig. 6. Percentage of hours inside the measured ranges of module temperature and in-plane irradiance for every location and technology.

number of hours for which the PV output depends on extrapolated values varies. Fig. 6 shows, for every location and technology, the percentage of the 8760 yearly hours that have corresponding conditions in the measured matrices described in Section 2.4.

Since the night hours are also included, the plotted percentages are all below 50%. The measured irradiance range is the same for all technologies (from 100 Wm^{-2} to 1000 Wm^{-2}), so the differences derive from the module temperature range used for each technology. The temperature set for the OPV goes from 15 °C to 45 °C, which explains, on one hand, the high percentages obtained at high latitudes, and on the other hand, the lower values at the lower latitudes, where the module temperature can go above 45 °C. For the location near the equator, these cases represent 12% of the yearly hours, when the average in-plane irradiance during these hours is 866 Wm^{-2}.

Similarly to the number of hours, Fig. 7 shows the percentage of the effective irradiance, G_{T_eff}, received during the whole year that is absorbed while the conditions of in-plane irradiance and temperature of the module fall inside the initial measured power matrix ranges. The percentages are mostly above 50%, with the exception of the location at 56°N for all technologies but the OPV and for the OPV at 24°N. This means that, in general, the estimated PV production depends more on the interpolated values than on the extrapolation procedure.

Fig. 8 shows the percentages of the yearly energy output that is produced with (G, T) conditions within the ones set in the measured matrices. The results from the 'Equation' and 'Matrix_extended' are

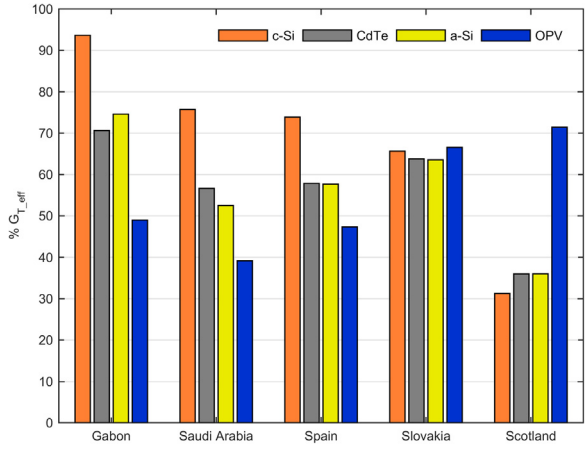

Fig. 7. Percentage of effective irradiance received while the module temperature and in-plane irradiance are inside the measured ranges for every location and technology.

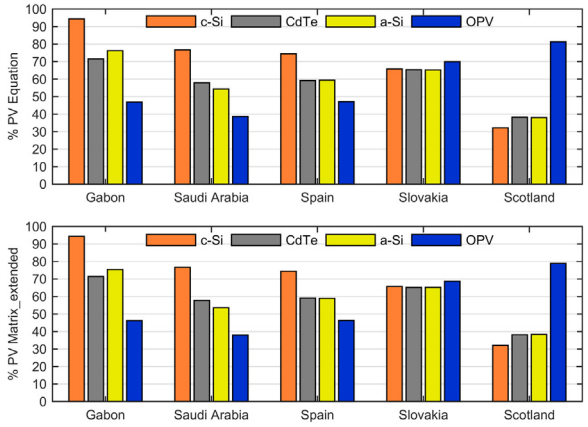

Fig. 8. Percentage of the yearly PV output estimated by the 'Equation' and 'Matrix_extended' methodologies that is produced while the module temperature and in-plane irradiance are inside the measured ranges for every location and technology.

presented.

The values shown in Fig. 8 do not change significantly between the two methodologies. For c-Si and CdTe modules, the percentages of the energy production estimated by interpolation of the measured values or obtained by the model equation differ at maximum by 0.18%. For the a-Si technology, the maximum difference of 0.82% is observed at 1°S. For the OPV device, the percentage deviations are higher, especially at higher latitudes with a difference of 1.18% and 2.41% at 48°N and 56°N, respectively, which means that the linear interpolation provides lower values than those estimated by the equation. For the OPV technology, the estimated PV output at lower latitudes depends significantly on extrapolated values ('Matrix_extended') as less than half of the production comes from conditions inside the ranges measured indoors in the initial matrix.

With exception of the organic device at the furthest north location, the percentage of irradiance received while conditions met the limits of the initial matrix is very similar to the PV output produced during the same hours. However, for the OPV at 56°N, 80% of the estimated energy output comes from moments inside those ranges, while the received irradiance in those hours represents the 70% of the yearly irradiation received. This means that a considerable percentage is produced outside the limits of the initial matrix, therefore depending on extrapolated values ('Matrix_extended') and situations where the device was not evaluated in indoor measurements, whose data were used to obtain the coefficients of the model (k_1 to k_6).

Notwithstanding, in general, the majority of the PV production comes from situations for which there are corresponding indoor measurements.

4.3.2. Impact of the inclination angle on the MPR values

All the results presented so far were obtained considering the modules tilted at every location with the optimum inclination angle so as to maximize the received irradiance (See Table 2). The same calculations were performed as well considering a fixed inclination angle of 20° at all the locations. The effect of the inclination angle, which affects the received irradiance and the temperature of the module, can be quantified by comparing the results of both analyses.

Moving the modules from the optimal inclination angle to a fixed one of 20° implies a variation of almost 20° for all locations but the one at 24°N, for which β_{opt} (°) is already 25°. The resulting variation of the yearly *MPR* values is lower than 0.5% in all the locations and for all the technologies. Using the optimal inclination angle does not result in higher *MPR* at all the locations. For instance, in the location near the equator, the *MPR* values for a fixed 20° inclination angle are slightly higher (less than 0.1%) than for the β_{opt}. This shows how by optimizing

Table 8
Average daytime ambient and module temperatures estimated with the c-Si and CdTe coefficients at every location. Variation, in %, of the yearly *MPR* values obtained for the organic technology when considering the two sets of temperature coefficients. Positive values mean that the c-Si coefficients result in higher *MPR* values.

Location	T_{amb} (°C)	T_{mod} c-Si (°C)	T_{mod} CdTe (°C)	Matrix (%)	Equation_limited (%)	Matrix_extended (%)	Equation (%)
Gabon	25.63	37.75	39.56	2.33	2.50	0.15	0.68
Saudi Arabia	27.96	40.18	41.97	0.95	1.01	0.07	0.55
Spain	20.21	34.60	36.74	1.91	2.03	0.06	0.60
Slovakia	14.26	23.05	24.35	0.85	0.91	− 0.03	0.14
Scotland	10.43	15.48	16.23	0.68	0.76	− 0.12	− 0.12

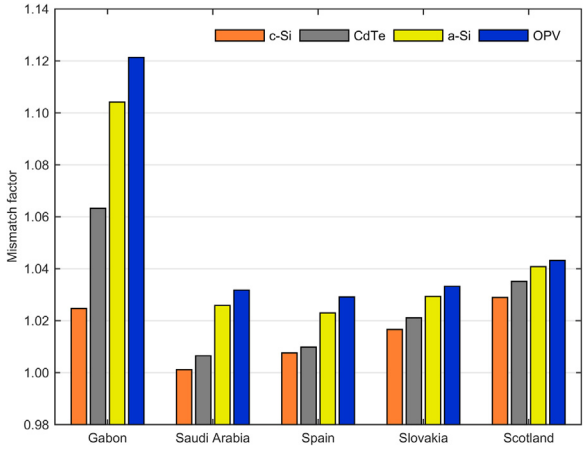

Fig. 9. Yearly mismatch factor of the four considered technologies at the five locations.

the inclination angle to maximize the in-plane irradiance does not guarantee a better performance as there are other factors, like spectral effects or temperature reached by the module that also affect the PV power output.

The differences presented here agree with [82] where the effect of the inclination angle on the *MPR* values was analysed at continental level. The average difference presented in that paper between the *MPR* values obtained for tilted planes at 20° and 40° was on average below 0.5%.

4.3.3. Impact of the temperature of the module on the MPR values of the OPV device

The temperature of the module, input data for the PV output model, was estimated using Faiman's model [74], which employs two coefficients (u_0 and u_1) that have not been defined for the OPV technology, yet. In this study, it was decided to estimate the temperature of the organic device by applying the coefficients for both the c-Si and the CdTe technologies. The results presented so far were obtained considering the coefficients from the c-Si technology. Here, a brief comparison between both cases is presented.

Applying the coefficients of the CdTe technology results in higher temperatures at all the locations. Focusing only on daytime temperatures, the increment in the temperature of the module relative to using the c-Si coefficients varies between 0.74 °C and 2.14 °C (see Table 8). The average daytime values of ambient and module's temperatures obtained from the two sets of coefficients are shown in Table 8.

To what extent these differences on the temperature of the module are reflected in the performance of the OPV technology, depends on the location and the methodology applied, as shown in Table 8. The table contains the difference, in percentage, of the yearly *MPR* values obtained applying the two sets of u_0 and u_1 coefficients (c-Si vs. CdTe). The performance is, in most cases, higher when using the c-Si coefficients, which results in lower module's temperatures, especially for the 'Matrix; and 'Equation_limited' methodologies. This may be explained by the fact that when using the CdTe coefficients, higher temperatures are obtained and some cases with low irradiance (and hence low efficiency) are “pushed into” the range of values of the initial matrix while some high-irradiance cases (with high efficiency) are "pushed out" of the range and therefore excluded. In fact, when the whole time series is considered ('Matrix_extended' and 'Equation') the differences in *MPR* values are below 1%.

At the furthest north location though, despite the fact that the module temperature from applying the Faiman's model c-Si coefficients is lower, the performance is slightly higher when the CdTe coefficients are applied.

4.3.4. Spectral response effect

The spectral mismatch factor, *MM*, calculated according to Eq. (6), accounts for the gain or loss in the absorbed irradiance relative to the STC conditions. The spectral distribution of the in-plane irradiance varies during the day and it is also affected by the atmospheric conditions. As a result, it is in general different from the STC spectrum, defined by the standard IEC 60904-3 [39].

Depending on the spectral irradiance distribution and the spectral responsivity of the active material of the PV modules (Fig. 1), the effectively absorbed irradiance may differ from that which would have been absorbed under the corresponding to the STC spectrum (same integrated irradiance value). The yearly *MM* values obtained from the different technologies at the locations analysed are plotted in Fig. 9.

The biggest gain from considering the real spectral irradiance distribution is observed at the location near the equator, where the spectral effect also varies more between the different technologies, because of the way the STC spectrum is defined. The calculated gain at this location goes from 2.5% for the c-Si module to 12% for the OPV technology. Generally, the narrower the spectral responsivity (see Fig. 1), the larger is the spectral effect [83,84]. The effect is strongest in areas like the tropics where the spectrum is depleted in the red and infrared, and where devices with a narrow spectral range in the blue part of the spectrum will have an advantage. This is also seen by the fact that the northernmost location also shows a significant spectral effect for all technologies, due to the high proportion of diffuse light which tends to have low red and infrared content. The positive mismatch factor equates to a direct proportional correction of the device current (or an effective irradiance factor is another way to considerate), therefore $MM > 1$ means more current and since current is directly proportional to power, better performance.

5. Conclusions

This paper presents a first approach to introduce an energy-based metric for the assessment of a newly developing PV technology in order to ultimately quantify the potential large-scale and long-term energy performance of the said technology. We accept there are significant assumptions in the application of the c-Si derived models, but it has been demonstrated that the results seem consistent both with measured data and the predicted output, which for the first time gives a mathematical tool for technology assessment to be applied to new PV materials.

The results presented here show that the performance of the OPV technology, in terms of the *MPR*, is similar to some of the most common technologies, and also that for some of the locations considered it may perform relatively better. These results give a positive indication of the fact that the OPV technology may, in some conditions, be a good alternative candidate for PV deployment, although further research for its stability has to be put in place.

Bearing in mind the degradation process observed on the OPV technology and the fact that the whole analysis presented here is based on a limited database of indoor measurements performed on one prototype mini-module, while standard commercially available PV modules are considered for the other technologies, the results and conclusions should be treated with caution. The present analysis is just a first approach to estimate the energy rating of this new technology, for which no outdoor performance data have been measured so far in our laboratory so as to conduct a more rigorous analysis.

We also note that some PV technologies show long-term variation in the module efficiency, which is especially the case for amorphous silicon technologies, even though this effect has not been taken into consideration in the present study. For the time being, we do not have sufficient information to confirm or exclude this for OPV. This will require development of models for the behaviour of these modules based on long time series of PV power measurements.

Besides the analysis of the PV performance of the OPV device in comparison to other technologies, the second main objective of this paper was the validation of the PV power output algorithm developed for silicon based modules to be applied to other technologies, including OPV. From the results of this work we can conclude that a better adjustment of the coefficients k_1 to k_6 of the PV power estimation model for the OPV devices is required. To this aim, additional measurements of OPV performance will be necessary, both indoors and outdoors. This is not an easy task as the OPV is rapidly evolving. However, new measurements of this technology are to be performed in our laboratory in the forthcoming months. We also conclude from this work the need for a better adjustment of the coefficients for the a-Si. However, the differences in the yearly *MPR* from 'Matrix_extended' and 'Equation' methodologies of 2% do not support the need to modify the formulation of the PV model for these two technologies. Probably redefining the coefficients would be enough. As for the CdTe technology, the differences are below 0.2% showing the validity of the silicon-based model for this other technology.

It has to be highlighted that the results of the OPV technology presented here are partially based on parameters that are specific to other technologies. Therefore, they may bias the comparison to a still undefined extent. For instance, the OPV mini-module used for this work is not yet in the full-size module production and we do not know how this technology would be encapsulated in the future, so the Faiman model temperature coefficients, u_0 and u_1, may differ from those used in the present study. However, the application of two different sets of coefficients has resulted only in small changes in the yearly *MPR* values, indicating that a change in their value should not significantly change the results presented. Notwithstanding, considering the noticeable effect that the temperature of the module has on its performance, once the technology becomes mature and modules become available, it would be important to define the proper coefficients u_0 and u_1 for the OPV technology.

The quality of the satellite-retrieved irradiance data and the PV power model applied in the present paper allowed us to consider the effect of the angle of incidence and the inclination of the module on the modules' performance. It was observed that these effects don't influence significantly the yearly *MPR* values. However, from our analysis we can conclude that the main effects influencing the *MPR* values and thus the energy production in real working conditions are two: the spectral effect, which by itself represents a significant gain with regard to the absorbed irradiance when considering the standard spectrum, especially for the location near the equator (up to 12% for the OPV devices, see Fig. 9). And the temperature reached by the modules which can positively enhance the power generation of the OPV devices in hot temperature conditions, in opposition to the effect of high temperatures observed in other technologies

Acknowledgements

The research work leading to this article was partly carried out within the EMRP ENG55 project "Towards an energy-based parameter for photovoltaic classification". The EMRP is jointly funded by the EMRP participating countries within EURAMET and the European Union.

Annex

Matrix extended

For every technology, the measured power matrix described in Section 2.4 has been extended both for the irradiance and the temperature values. The in-plane irradiance range was increased to cover from 50 Wm^{-2} to 1200 Wm^{-2} at 50 Wm^{-2} steps, while the module's temperature has been defined from − 15 °C to 100 °C at 5 °C steps. In order to obtain the PV output values at these levels of G_{T_eff} and T_{mod}, interpolation and extrapolation procedures have been applied to the original measurements.

The whole procedure is applied to the efficiencies values, *eff*, and not to the maximum power values. The efficiency is calculated according to Eq. (A1).

$$eff\,(G_{T_eff},\ T_{mod}) = P(G_{T_eff},\ T_{mod}) \cdot \frac{1000}{G_{T_eff}} \tag{A1}$$

where P is the measured P_{max} value at the in-plane irradiance value G_{T_eff} and module temperature, T_{mod}.

Using the efficiency values, the extended matrix is calculated as follows:

Firstly, the new efficiency values are calculated for every level of temperature separately. Using the efficiency values at the initial levels of irradiance, a linear interpolation is applied to calculate the efficiency at the new levels of irradiance, added every 50 Wm^{-2} among those of the measured power matrix. By doing this, the irradiance range from 100 Wm^{-2} to 1000 Wm^{-2} is filled with efficiency values every 50 Wm^{-2}.

At the following step, the efficiency is calculated for the irradiance levels outside the initial interval, in order to cover the full range from 50 Wm^{-2} to 1200 Wm^{-2}. This is done by using a linear extrapolation applied to the closest initial efficiency values. For instance, in order to estimate the value at 50 Wm^{-2}, data from 100 Wm^{-2} and 200 Wm^{-2} are used. For higher irradiances, depending on the technology, the data measured under 1000 Wm^{-2} and 900 Wm^{-2} or 800 Wm^{-2} is used.

Up to this point, there are efficiency values every 50 Wm^{-2} between 50 Wm^{-2} and 1200 Wm^{-2}, at the same temperatures of the module shown in Table 3.

Working now with the efficiency values at every level of irradiance separately, the efficiency is calculated for the new temperatures inside the initial T_{mod} range by applying a linear interpolation within the said interval of temperature. The efficiency is calculated every 5 °C. For instance, for

the c-Si technology, efficiencies are calculated at 30, 40, 50 and 55 °C, since the initial matrix has data at 25, 35, 45 and 60 °C. For the OPV device, this interpolation is not necessary as the PV output was originally measured every 5 °C. However, the covered temperatures go from 15 °C to 45 °C, so the extrapolation is required to extend the initial matrix.

Considering the efficiency values at the three lowest temperatures of the initial ones, new values are linearly calculated every 5 °C until −15 °C. Similarly, but using the efficiency values of the three highest measured temperatures, new efficiency values are calculated up to 100 °C.

Once the extended matrix of efficiency values is obtained, it is transformed to power values using Eq. (A2).

$$P(G_{T_eff},\ T_{mod}) = eff\,(G_{T_eff},\ T_{mod}) \bullet \frac{G_{T_eff}}{1000} \tag{A2}$$

With this procedure, for every technology there is an extended matrix of power output from 50 Wm^{-2} to 1200 Wm^{-2} at 50 Wm^{-2} steps, and from − 15 °C to 100 °C at 5 °C steps.

These new matrices will be used to estimate the power output of the different technologies for the hourly values of the initial time series with the defined methodology 'Matrix_extended' (See Section 3.7).

References

[1] Jäger-Waldau A. PV Status Report; EUR 28159 EN, ⟨http://dx.doi.org/10.2790/682995⟩; 2016.
[2] Brown GF, Wu J. Third generation photovoltaics. Laser Photonics Rev 2009;3:394–405.
[3] Green MA Third generation photovoltaics: assessment of progress over the last decade. In: Proceedings of the 34th IEEE Photovoltaic Spec. Conference, June 7-12, 2009, Philadelphia, PA, p. 000146–000149.
[4] Chang NL, Ho-Baillie AWY, Vak D, Gao M, Green MA, Egan RJ. Manufacturing cost and market potential analysis of demonstrated roll-to-roll perovskite photovoltaic cell processes. Sol Energy Mater Sol Cells 2018;174:314–24.
[5] Lizin S, Van Passel S, De Schepper S, Vranken L. The future of organic photovoltaic solar cells as a direct power source for consumer electronics. Sol Energy Mater Sol Cells 2012;103:1–10.
[6] European Photovoltaic Industry Association (EPIA). Global Market Outlook for Photovoltaics2014-2018; 2014.
[7] Lacerda JS, van den Bergh JCJM. Diversity in solar photovoltaic energy: implications for innovation and policy. Renew Sustain Energy Rev 2016;54:331–40.
[8] Carlé JE, Helgesen M, Hagemann O, Hösel M, Heckler IM, Bundgaard E, Gevorgyan SA, Søndergaard RR, Jørgensen M, García-Valverde R, Chaouki-Almagro S, Villarejo JA, Krebs FC. Overcoming the scaling lag for polymer solar cells. Joule 2017;1(2):274–89.
[9] Jørgensen M, Carlé JE, Søndergaard RR, Lauritzen M, Dagnæs-Hansen NA, Byskov SL, Andersen TR, Larsen-Olsen TT, Böttiger APL, Andreasen B, Fu L, Zuo L, Liu Y, Bundgaard E, Zhan X, Chen H, Krebs FC. The state of organic solar cells – a meta analysis. Sol Energy Mater Sol Cells 2013;119:84–93.
[10] Gong J, Sumathy K, Qiao Q, Zhou Z. Review on dye-sensitized solar cells (DSSCs): advanced techniques and research trends. Renew Sustain Energy Rev 2017;68(1):234–46.
[11] Best Research-Cell Efficiencies, National Renewable Energy Laboratory. ⟨http://www.nrel.gov/pv/assets/images/efficiency-chart.png⟩; [accessed 31 March 2017].
[12] Green MA, Emery K, Hishikawa Y, Warta W, Dunlop ED, Levi DH, et al. Solar cell efficiency tables (version 50). Prog Photovolt Res Appl 2017;25(7):668–76.
[13] Habibi M, Zabihi F, Ahmadian-Yazdi MR, Eslamian M. Progress in emerging solution-processed thin film solar cells – Part II: perovskite solar cells. Renew Sustain Energy Rev 2016;62:1012–31.
[14] Kumavat PP, Sonar P, Dalal DS. An overview on basics of organic and dye sensitized solar cells, their mechanism and recent improvements. Renew Sustain Energy Rev 2017;78:1262–87.
[15] Mehmood U, Al-Ahmed A, Afzaal M, Al-Sulaiman FA, Daud M. Recent progress and remaining challenges in organometallic halides based perovskite solar cells. Renew Sustain Energy Rev 2017;78:1–14.
[16] Assadi MK, Bakhoda S, Saidur R, Hanaei H. Recent progress in perovskite solar cells. Renew Sustain Energy Rev. In press, corrected proof, Available online 29. ⟨https://doi.org/10.1016/j.rser.2017.06.088⟩; June 2017.
[17] Kumar M, Kumar A. Performance assessment and degradation analysis of solar photovoltaic technologies: a review. Renew Sustain Energy Rev 2017;78:554–87.
[18] Grossiord N, Kroon JM, Andriessen R, Blom PWM. Degradation mechanism in organic photovoltaic devices. Org Electron 2012;13(3):432–56.
[19] Espinosa N, Zimmermann Y-S, dos Reis Benatto GA, Lenz M, Krebs FC. Outdoor fate and environmental impact of polymer solar cells through leaching and emission to rainwater and soil. Energy Environ Sci 2016;9(5):1674–80.
[20] Córcoles L, Abad J, Padilla J, Urbina A. Wavelength influence on the photodegradation of P3HT:PCBM organic solar cells. Sol Energy Mater Sol Cells 2015;141:423–8.
[21] Zimmermann Y-S, Schäffer A, Hugi C, Fent K, Corvini PFX, Lenz M. Organic photovoltaics: potential fate and effects in the environment. Environ Int 2012;49:128–40.
[22] Ibn-Mohammed T, Koh SCL, Reaney IM, Acquaye A, Greenough R. Perovskite solar cells: an integrated hybrid lifecycle assessment and review in comparison with other photovoltaic technologies. Renew Sustain Energy Rev 2017;80:1321–44.
[23] Mesquita I, Andrade L, Mendes A. Perovskite solar cells: materials, configurations and stability. Renew. Sustain Energy. Rev. 2018;82:2471–89.
[24] Wang D, Wright M, Elumalai NK, Uddin A. Stability of perovskite solar cells. Sol Energy Mater Sol Cells 2016;147:255–75.
[25] Asghar MI, Zhang J, Wang H, Lund PD. Device stability of perovskite solar cells – a review. Renew Sustain Energy Rev 2017;77:131–46.
[26] Djurisic AB, Liu FZ, Tam HW, Wong MK, Ng A, Surya C, Chen W, He ZB. Perovskite solar cells – an overview of critical issues. Prog Quant Electron 2017;53:1–37.
[27] Nelson J. Organic photovoltaic films. Curr Opin Sol State Mater Sci 2002;6(1):87–95.
[28] Spanggaard H, Krebs FC. A brief history of the development of organic and polymeric photovoltaics. Sol Energy Mater Sol Cells 2004;83:125–46.
[29] Yeh N, Yeh P. Organic solar cells: their developments and potentials. Renew Sustain Energy Rev 2013;21:421–31.
[30] Liu X, Chen H, Tan S. Overview of high-efficiency organic photovoltaic materials and devices. Renew Sustain Energy Rev 2015;52:1527–38.
[31] Wang Q, Xie Y, Soltani-Kordshuli F, Eslamian M. Progress in emerging solution-processed thin film solar cells – Part I: polymer solar cells. Renew Sustain Energy Rev 2016;56:347–61.
[32] Walker B, Choi H, Kim JY. Interfacial engineering for highly efficient organic solar cells. Curr Appl Phys 2017;17:370–91.
[33] Menke SM, Ran NA, Bazan GC, Friend RH. Understanding energy loss in organic solar cells: toward a new efficiency regime. Joule 2017. http://dx.doi.org/10.1016/j.joule.2017.09.020.
[34] Holliday S, Li Y, Luscombe CK. Recent advances in high performance donor-acceptor polymers for organic photovoltaics. Prog Polym Sci 2017;70:34–51.
[35] Scharber MC, Sariciftci NS. Efficiency of bulk-heterojunction organic solar cells. Prog Polym Sci 2013;38:1929–40.
[36] Green MA, Emery K, King DL, Hishikawa Y, Warta W. Solar cell efficiency tables (version 28). Prog Photovolt Res Appl 2006;14:455–61.
[37] Heeger AJ. Solar cells and light-emitting field effect transistors: recent progress in Santa Barbara, Materials and Basic Research Needs for Solar Energy Conversion. In: Proc of Symposium FF at the 2006 Materials Research Society Spring Meeting, San Francisco, California, volume 945; April 17-21, 2006.
[38] Mori S, Oh-oka H, Nakao H, Gotanda T, Nakano Y, Jung H. et al. Organic photovoltaic module development with inverted device structure. In: Materials Research Society Proc 2015: ⟨http://dx.doi.org/10.1557/opl.2015.540⟩; 1737.
[39] IEC 60904-3. Photovoltaic devices – Part 3: Measurement principles for terrestrial photovoltaic (PV) solar devices with reference spectral irradiance data. ⟨isbn:2-8318-9705-X⟩.
[40] IEC 60904-2. Photovoltaic devices – Part 2: Requirements for reference solar devices. ⟨isbn:9780580859717⟩.
[41] Katz EA, Faiman D, Tuladhar SM, Kroon JM, Wienk MM, Fromherz T, Padinger F, Brabec CJ, Sariciftci NS. Temperature dependence for the photovoltaic device parameters of polymer-fullerene solar cells under operating conditions. J Appl Phys 2001;90:5343.
[42] Riedel I, Parisi J, Dyakonov V, Lutsen L, Vanderzande D, Hummelen JC. Effect of temperature and illumination on the electrical characteristics of polymer–fullerene bulk-heterojunction solar cells. Adv Funct Mater 2004;14:38–44.
[43] Tromholt T, Katz EA, Hirsch B, Vossier A, Krebs FC. Effects of concentrated sunlight on organic photovoltaics. Appl Phys Lett 2010;96:073501.
[44] Bagienski W, Gupta MC. Temperature dependence of polymer/fullerene organic solar cells. Sol Energy Mater Sol Cells 2011;95(3):933–41.
[45] Burlingame Q, Zanotti G, Ciammaruchi L, Katz EA, Forrest SR. Outdoor operation of small-molecule organic photovoltaics. Org Electron 2017;41:274–9.
[46] Zhang Y, Yi H, Iraqi A, Kingsley J, Buckley A, Wang T, Lidzey DG. Comparative indoor and outdoor stability measurements of polymer based solar cells. Sci Rep 2017;7:1305.
[47] Krebs FC, Espinosa N, Hösel M, Søndergaard RR, Jørgensen M. 25th anniversary article: rise to power—OPV-based solar parks. Adv Mater 2014;26:29–39.
[48] Bristow N, Kettle J. Outdoor organic photovoltaic module characteristics: benchmarking against other PV technologies for performance, calculation of Ross coefficient and outdoor stability monitoring. Sol Energy Mater Sol Cells 2018;175:52–9.
[49] Bristow N, Kettle J. Outdoor performance of organic photovoltaics: diurnal analysis, dependence on temperature, irradiance, and degradation. J Renew Sustain Energy 2015;7:013111.
[50] Katz EA, Gevorgyan S, Orynbayev MS, Krebs FC. Out-door testing and long term stability of plastic solar cells. Eur Phys J Appl Phys 2006;36:307–11.
[51] Angmo D, Krebs FC. Over 2 years of outdoor operational and storage stability of

ITO-free, fully roll-to-roll fabricated polymer solar cell modules. Energy Technol 2015;3:774–83.
[52] Søndergaard RR, Makris T, Lianos P, Manor A, Katz EA, Gong W, Tuladhar SM, Nelson J, Tuomi R, Sommeling P, Veenstra C, Rivaton A, Dupuis A, Teran-Escobar G, Lira-Cantu M, Sapkota SB, Zimmermann B, Würfel U, Krebs FC. The use of polyurethane as encapsulating method for polymer solar cells—An inter laboratory study on outdoor stability in 8 countries. Sol Energy Mater Sol Cells 2012;99:292–300.
[53] Emmott CFM, Moia D, Sandwell P, Ekins-Daukes N, Hösel M, Lukoschek L, Amarasinghe C, Krebs FC. In-situ, long-term operational stability of organic photovoltaics for off-grid applications in Africa. Sol Energy Mater Sol Cells 2016;149:284–93.
[54] Angmo D, Sommeling PM, Gupta R, Hösel M, Gevorgyan SA, Kroon JM, Kulkarni GU, Krebs FC. Outdoor operational stability of indium-free flexible polymer solar modules over 1 year studied in India, Holland, and Denmark. Adv Eng Mater 2014;16(8):976–87.
[55] IEC 61853-1. Photovoltaic (PV) module performance testing and energy rating – Part 1: Irradiance and temperature performance measurements and power rating.
[56] IEC 61853-2. Photovoltaic (PV) module performance testing and energy rating – Part 2: Spectral responsivity, incidence angle and module operating temperature measurements.
[57] Huld T, Friesen G, Skoczek A, Dunlop ED. A power-rating model for crystalline silicon PV modules. Sol Energy Mater Sol Cells 2011;95(12):3359–69.
[58] Suri M, Huld TA, Dunlop ED. PV-GIS: a web-based solar radiation database for the calculation of PV potential in Europe. Int J Sust Energy 2005;24(2):55–67.
[59] Mueller RW, Matsoukas C, Gratzki A, Behr HD, Hollmann R. The CM-SAF operational scheme for the satellite based retrieval of solar surface irradiance – A LUT based eigenvector hybrid approach. Remote Sens Environ 2009;113:1012–24.
[60] Mueller R, Behrendt T, Hammer A, Kemper A. A new algorithm for the satellite-based retrieval of solar surface irradiance in spectral bands. Rem Sens 2012;4:622–47.
[61] Kato S, Ackerman TP, Mather JH, Clothiaux EE. The k-distribution method and correlated-k approximation for a short-wave radiative transfer. J Quant Spectrosc Radiat Transf 1999;62(1):109–21.
[62] Dee DP, Uppala SM, Simmons AJ, Berrisford P, Poli P, Kobayashi S, et al. The ERA-Interim reanalysis: configuration and performance of the data assimilation system. Q J R Meteorol Soc 2011;137(656):553–97.
[63] IEC 60904-60908. Photovoltaic devices – Part 8: Measurement of spectral responsivity of a photovoltaic (PV) device.
[64] Bahrs U, Zaaiman W, Mertens M, Ossenbrink H. Automatic large area spectral response facility. In: Proc. 14th European Photovoltaic Solar Energy Conference, EU PVSEC, June 30-July 4, Barcelona, Spain, 1997, p. 2296–2298.
[65] Ebner B, Agostinelli G, Dunlop ED Automated absolute spectral response characterization for calibration of secondary standards. In: Proc. 16th European Photovoltaic Solar Energy Conference, EU PVSEC, May 1-5, 2000, Glasgow, UK, p. 2202–2205.
[66] Bardizza G, Salis E, Dunlop ED Testing an organic photovoltaic device at different temperature and irradiance conditions: a first attempt of a power matrix study on OPV mini-modules. 'Submitted to a Journal'.
[67] Nikolaeva-Dimitrova M, Kenny RP, Dunlop ED, Pravettoni M. Seasonal variations on energy yield of a-Si, hybrid, and crystalline Si PV modules. Prog Photovolt Res Appl 2010;18(5):311–20.
[68] Kenny RP, Viganó D, Salis E, Bardizza G, Norton M, Müllejans H, et al. Power rating of photovoltaic modules including validation of procedures to implement IEC 61853-1 on solar simulators and under natural sunlight. Prog Photovolt Res Appl 2013;21(6):1384–99.
[69] Muneer T. Solar radiation model for Europe. Build Serv Eng Res Technol 1990;11(4):153–63.
[70] Gracia Amillo A, Huld T. Performance comparison of different models for the estimation of global irradiance on inclined surfaces, Technical Report: European Commission, Joint Research Centre; 2013. 〈http://re.jrc.ec.europa.eu/pvgis/doc/report/ReqNO_JRC81902_Report.pdf〉 [accessed 31 March 2017].
[71] Martin N, Ruiz JM. Calculation of the PV modules angular losses under field conditions by means of an analytical model. Sol Energy Mater Sol Cells 2001;70(1):25–38.
[72] Martin N, Ruiz JM. Corrigendum to "Calculation of the PV modules angular losses under field conditions by means of an analytical model", [Sol Energy Mater Sol Cells 2001;70(1):25-38]. Sol Energy Mater Sol Cells 2012;110:154.
[73] IEC 60904-60907. Photovoltaic devices – Part 7: Computation of the spectral mismatch correction for measurements of photovoltaic devices. 〈isbn:978-2-88910-324-9〉.
[74] Faiman D. Assessing the outdoor operating temperature of photovoltaic modules. Prog Photovolt Res Appl 2008;16(4):307–15.
[75] Dirnberger D, Müller B, Reise C. PV module energy rating: opportunities and limitations. Prog Photovolt Res Appl 2015;23:1754–70.
[76] Kaldellis JK, Kapsali M, Kavadias KA. Temperature and wind speed impact on the efficiency of PV installations. experience obtained from outdoor measurements in Greece. Renew Energy 2014;66:612–24.
[77] Koehl M, Heck M, Wiesmeier S, Wirth J. Modeling of the nominal operating cell temperature based on outdoor weathering. Sol Energy Mater Sol Cells 2011;95(7):1638–46.
[78] Dittmann S, Friesen G, Williams SR, Betts TR, Gottschalg R, Beyer HG, et al. Results of the 3rd modelling round robin within the European project PERFORMANCE – Comparison of module energy rating methods. In Proc 25th European Photovoltaic Solar Energy Conference, EU PVSEC, September 6-10, 2010, Valencia, Spain, p. 4333–4338.
[79] Huld T, Dunlop E, Beyer HG, Gottschalg R. Data sets for energy rating of photovoltaic modules. Sol Energy 2013;93:267–79.
[80] Cañete C, Carretero J, Sidrach-de-Cardona M. Energy performance of different photovoltaic module technologies under outdoor conditions. Energies 2014;65:295–302.
[81] Makrides G, Zinsser B, Phinikarides A, Schubert M, Georghiou GE. Temperature and thermal annealing effects on different photovoltaic technologies. Renew Energy 2012;43:407–17.
[82] Huld T, Gracia Amillo AM, Estimating PV. module performance over large geographical regions: the role of irradiance, air temperature, wind speed and solar spectrum. Energies 2015;8(6):5159–81.
[83] Dirnberger D, Blackburn G, Müller B, Reise C. On the impact of solar spectral irradiance on the yield of different PV technologies. Sol Energ Mater Sol Cells 2015;132:431–42.
[84] Ishii T, Otani K, Itagaki A, Utsunomiya K. A simplified methodology for estimating solar spectral influence on photovoltaic energy yield using average photon energy. Energy Sci Eng 2013;1:18–26.